

# **FINITE ELEMENT ANALYSIS OF DUCTILE FAILURE IN STRUCTURAL STEEL SUBJECTED TO MULTIAXIAL STRESS STATES AND HIGH STRAIN RATES**

*T. Børvik<sup>1</sup>, O.S. Hopperstad<sup>1</sup>, T. Berstad<sup>2</sup>, S. Dey<sup>1</sup> and M. Langseth<sup>1</sup>*

*1) Structural Impact Laboratory - SIMLab*

*Department of Structural Engineering*

*Norwegian University of Science and Technology*

*Rich. Birkelandsvei 1a, N-7491 Trondheim, Norway*

*E-mail: [tore.borvik@bygg.ntnu.no](mailto:tore.borvik@bygg.ntnu.no)*

*2) Livermore Software Technology Corporation - LSTC*

*7374 Las Positas Road, Livermore, CA 94550, USA*

## Abstract

Notched specimens of the structural steel Weldox 460 E have been tested at high strain rates in a Split Hopkinson Tension Bar. The aim was to study the combined effects of strain rate and stress triaxiality on the strength and ductility of the material. It is further considered important to obtain experimental data that may be used in validation of constitutive relations and fracture criteria. The force and elongation of the specimens were measured continuously by strain gauges on the half-bars, while the true fracture strain was calculated based on measurements of the fracture area. Optical recordings of the notch deformation were obtained using a digital high-speed camera system. Using image processing of the digital images, it was possible to estimate the true strain versus time at the minimum cross-section in the specimen. The ductility of the material was found to depend considerably on the stress triaxiality. Non-linear finite element analyses of the notched tensile specimens at high strain rates have been carried out using LS-DYNA. A computational material model including viscoplasticity and ductile damage has been implemented in LS-DYNA and determined for Weldox 460 E steel. The aim of the numerical simulations was to assess the validity of the material model by comparison with the available experimental results.

## Introduction

Constitutive relations for materials at high strain rates are important in many industrial applications, such as crashworthiness, structural impact and plastic forming operations. Since high rate loading conditions may lead to adiabatic temperature rise in the material, it is necessary to allow for high strain rates and elevated temperatures in the constitutive model. Furthermore, constitutive relations for metals under impact loading are normally empirical or semi-empirical, and thus extensive experimental investigations are typically needed to determine the material constants with the required accuracy.

The aim of the current study was to obtain experimental data that can be used to validate constitutive relations and fracture criteria for a structural steel at impact rates of strain, and to increase our understanding of the material behaviour under such loading conditions. To this end, notched axisymmetric specimens of Weldox 460 E steel with three different notch root radii were tested in tension at two strain rates to give the combined effect of strain rate and stress triaxiality on the material behaviour. The tests were performed in a Split Hopkinson Tension Bar, using a digital high-speed camera system to record the local deformation in the notch. Experimental results are presented and used to validate a computational material model of viscoplasticity and ductile damage. The material model has been implemented in LS-DYNA and used with success in simulations of projectile penetration in Weldox 460 E steel plates, see Børvik et al [1]-[5] for details.

## Definition of stress and strain variables

The equivalent stress  $\sigma_{eq}$  is defined in terms of the principal stress components  $\sigma_1$ ,  $\sigma_2$  and  $\sigma_3$  as (Hancock and Mackenzie [6])

$$\sigma_{eq} = \left[ \frac{1}{2} \{ (\sigma_1 - \sigma_2)^2 + (\sigma_2 - \sigma_3)^2 + (\sigma_3 - \sigma_1)^2 \} \right]^{1/2}$$

The elastic region in the stress space is defined by the yield surface  $\sigma_{eq} = Y$ , where  $Y$  is the current macroscopic yield stress of the material. The accumulated plastic strain  $p$  is defined by its rate  $\dot{p}$  as

$$\dot{p} = \left[ \frac{2}{9} \{ (\dot{\epsilon}_1^p - \dot{\epsilon}_2^p)^2 + (\dot{\epsilon}_2^p - \dot{\epsilon}_3^p)^2 + (\dot{\epsilon}_3^p - \dot{\epsilon}_1^p)^2 \} \right]^{1/2}$$

where  $\dot{\epsilon}_1^p$ ,  $\dot{\epsilon}_2^p$  and  $\dot{\epsilon}_3^p$  are the principal components of the plastic strain rate field. The equivalent stress and the accumulated plastic strain  $p$  are connected through a constitutive relation,  $\sigma_{eq} = f(p, \dot{p}, T)$ , where  $T$  is the temperature. It is assumed that the yielding and plastic flow is independent of the mean stress  $\sigma_m$ , which is defined by

$$\sigma_m = \frac{1}{3} (\sigma_1 + \sigma_2 + \sigma_3)$$

The equivalent stress  $\sigma_{eq}$  and mean stress  $\sigma_m$  are combined into a non-dimensional parameter  $\sigma_m/\sigma_{eq}$  that characterises the stress state and represents a measure of the stress triaxiality.

## Computational material model

The constitutive relations for metallic materials under impact loading are normally empirical or semi-empirical, defining the equivalent stress  $\sigma_{eq}$  in terms of accumulated plastic strain  $p$ , plastic strain rate  $\dot{p}$  and temperature  $T$ . Two important constitutive relations, which are frequently used for impact analysis, have been proposed by Johnson and Cook [7] and Zerilli and Armstrong [8]. Owing to its simple identification and widespread use for impact problems, the former constitutive equation has been adopted in the present investigation. The Johnson-Cook relation reads [7]

$$\sigma_{eq} = (A + Bp^n)(1 + C \ln \dot{p}^*)(1 - T^{*m})$$

where there are five material constants  $A$ ,  $B$ ,  $C$ ,  $n$  and  $m$ . The dimensionless plastic strain rate is given by  $\dot{p}^* = \dot{p}/\dot{p}_0$ , where  $\dot{p}_0$  is a user-defined reference strain rate. The homologous temperature  $T^*$  is defined as  $T^* = (T - T_r) / (T_m - T_r)$ , where  $T$  is the absolute temperature, and suffixes  $r$  and  $m$  indicate room and melting temperature, respectively (Harding [9]). It is convenient to modify the Johnson-Cook equation for more efficient implementation into FE codes, and the result is (Camacho and Ortiz [10])

$$\sigma_{eq} = (A + Bp^n)(1 + \dot{p}^*)^C(1 - T^{*m})$$

The computational fracture model of Johnson and Cook [11] is based on damage accumulation, and has the basic form

$$D = \sum D_c \frac{\Delta p}{p_f}$$

where  $D$  is the damage to a material element,  $\Delta p$  is the increment of accumulated plastic strain (that occurs during an integration cycle), and  $p_f$  is the accumulated plastic strain to failure under the current conditions of stress triaxiality, strain rate and temperature. Failure (or element erosion) occurs when  $D = D_c$ . In the original fracture model of Johnson and Cook the critical damage was equal to unity. For proportional loading with constant stress triaxiality Hancock and Mackenzie [6] proposed a fracture strain defined by

$$p_f = p_n + \alpha \exp[-3/2 \cdot \sigma_m / \sigma_{eq}]$$

where  $p_n$  is a nucleation strain and  $\alpha$  is a material characteristic. The criterion was partly based on the Rice-Tracey void growth equation (Rice and Tracy [12]) and partly on experimental results. Johnson and Cook [11] extended this fracture criterion by including effects of strain rate and temperature

$$p_f = [D_1 + D_2 \exp(D_3 \sigma_m / \sigma_{eq})][1 + D_4 \ln \dot{p}^*][1 + D_5 T^*]$$

Also the Johnson-Cook fracture strain is modified according to the expression proposed by Camacho and Ortiz [10]

$$p_f = [D_1 + D_2 \exp(D_3 \sigma_m / \sigma_{eq})][1 + \dot{p}^*]^{D_4} [1 + D_5 T^*]$$

where  $D_1, \dots, D_5$  are material constants.

The constitutive relation and the fracture criterion may be coupled to account for damage softening, using the principles of effective stress and strain equivalence (Lemaitre [13]). The result is that the constitutive relation can be rewritten as

$$\sigma_{eq} = (1 - D)(A + Br^n)(1 + \dot{r}^*)^C(1 - T^{*m})$$

where  $r$  is the damage accumulated plastic strain, defined in rate form by  $\dot{r} = (1 - D)\dot{p}$ , and  $\dot{r}^* = \dot{r}/\dot{p}_0$  is the dimensionless plastic strain rate for the damaged material. It is referred to Børvik et al [1] for details about this coupled model of viscoplasticity and ductile damage based on the constitutive relation and fracture model proposed by Johnson and Cook [7][11].

In the present study, the material model is used for adiabatic conditions, and it is thus necessary to estimate the increase in temperature due to plastic work. The temperature increase because of adiabatic heating is calculated as

$$\Delta T = \int_0^p \chi \frac{\sigma_{eq}}{\rho C_p} dp$$

where  $\rho$  is the density,  $C_p$  is the specific heat and  $\chi$  is the proportion of plastic work converted into heat. In this study,  $\chi$  is assumed to be constant and equal to 0.9.

## Experiments

The notched specimens were made from a 12 mm thick plate of Weldox 460 E steel and tested in the as-received condition. Weldox 460 E is a thermo-mechanically rolled ferritic structural steel offering high strength combined with a high degree of ductility. All specimens were taken parallel to the rolling direction of the steel plate, since prior tests indicate that the material is approximately isotropic. The geometry and dimensions of the notched specimens are given in Figure 1. Tests were performed for three different notch root radii  $R_0$  equal to 0.4 mm, 0.8 mm and 2 mm. Two levels of loading rate were applied, defined by a pre-loading force  $N_0$  equal to 20 kN and 40 kN. In this paper, only tests with a pre-load of 20 kN will be considered. For each of the six combinations, four parallel tests were performed. One additional test was performed for the combination  $R_0=0.8$  mm and  $N_0=20$  kN, so that the total number of tests was 25.

The tensile tests were performed in a Split Hopkinson Tension Bar (Albertini and Montagnani [14]). The test apparatus consists of two half-bars called the input bar and output bar, and the specimen is inserted between these bars. Elastic energy is stored in a pre-stressed loading device, which is the solid continuation of the input bar. By rupturing a brittle intermediate piece, a tension wave with a rise-time of 50  $\mu$ s is transmitted along the input bar and loads the specimen to fracture. The strain rate is changed by varying the pre-loading force  $N_0$  of the loading device and thus the stored elastic energy.

According to the theory of one-dimensional elastic wave propagation in circular rods (Kolsky [15]), the elastic stress wave propagates along the input bar with a constant velocity and shape. When the incident pulse reaches the specimen, it is partly reflected by the interface between the input bar and the specimen, and partly transmitted through the specimen and into the output bar. The relative amplitudes of the incident, reflected and transmitted pulses depend on the mechanical properties of the specimen. It is assumed that the specimen, which is short relative to the input and output bars, reaches a state of force equilibrium after numerous reflections of elasto-plastic waves inside it. Strain gauges are placed on the input and output bars at equal distances from the specimen and these are used to measure the elastic deformations versus time in the half-bars caused by the incident, reflected and transmitted pulses. The measurements are subsequently used to calculate the elongation, the force and the rate of elongation of the specimen, using one-dimensional elastic wave theory (Kolsky [15]).

In some of the parallel tests, a digital high-speed camera system was used to obtain optical recordings of the notch deformation. The purpose of the set-up for optical measurements was to capture images of the specimen during deformation and to derive the diameter reduction as a function of time. For each test, the specimen diameter was calculated for a pre-test calibration image and 15 test images. The calculated diameters from the test images were then divided by the diameter of the calibration image to achieve a relative diameter. The duration of the experiment varied with the change in specimen geometry and pre-loading force. Therefore, it was attempted to adjust the interval between the images so that the first image was taken just before the pulse reached the specimen and the final image was taken just after complete failure.

Some results from the Split Hopkinson Tension Bar tests are presented in Figure 2 in terms of typical elongation-time curves and force-time curves for the three different notch radii at 20 kN pre-loading force. These particular experiments will be used in the following validation study with LS-DYNA.

## Numerical simulations

The finite element code LS-DYNA [16] was used in the analysis of the impact tests. The finite element models of the notched specimens are shown in Figure 3. The specimens were modelled using four-node axisymmetric elements with one-point integration and stiffness-based hourglass control. Introductory simulations were performed to establish the mesh density defined in Figure 3, taking into account the accuracy of the stress state predictions at the centre of the test specimen and the computational efficiency. The loading was defined by prescribing the elongation of the left specimen end against time, using the measured elongation-time curves from Figure 2, while the right end was fixed (see Figure 3).

The computational material model of viscoplasticity and ductile damage was used in the simulations. In a previous study (Børvik et al [1]), the material model was determined based on experimental data from quasi-static tests on smooth and notched specimens at room temperature, high strain rate tests on smooth specimens at room temperature, and quasi-static tests on smooth specimens at elevated temperatures. The identification method used was based on simple analytical considerations. The material constants for Weldox 460 E are compiled in Table 1. Note that in the simulations element erosion was used to remove elements that reached the critical damage level DC. This approach makes it possible to predict failure of the notched specimens.

## Results and discussion

Typical force-elongation curves from tests with pre-load 20 kN are compiled in Figure 4 and compared with corresponding curves obtained in the LS-DYNA simulations. Figure 4(a) demonstrates that severe oscillations occur in the numerical force-time curves, while this is not the case for the experimental curves. The reason is that only the specimen was modelled in the numerical model and it follows that the calculated force is disturbed by an elastic wave that propagates along the specimen length and is reflected from the specimen ends. The wavelength of the oscillations agrees with the time it takes for the elastic wave to travel twice from one side of the specimen to the other. In order to get rid of the force oscillations, the force signals from the numerical simulations were filtered using a cosine filter with cut-off frequency of 10000 Hz. The unfiltered and filtered signals from the simulation with notch radius 0.4 mm are compared in Figure 4(a). The comparison of tests and simulations in Figure 4(b)-(d) shows that the finite element model is capable of describing both the force-elongation curves and the ductile failure of the notched specimens with good accuracy when considering the complexity of the material tests. It should also be kept in mind that some scatter was found in the experimental data.

Diameter reduction and strain versus time from experiments and simulations are presented in Figure 5(a)-(c). The average strain at the minimum cross-section of the notched specimens in the tests and simulations was calculated as (Hancock and Mackenzie [6])

$$\varepsilon = 2 \ln(d_0 / d)$$

where  $d$  is the diameter of the minimum cross-section and  $d_0$  is the initial value of  $d$ . The elastic strains are assumed to be negligible compared with the plastic strains, so that no distinction needs to be made between plastic strains and total strains. In the experiments, the current value of  $d$  was based on the digital high-speed camera measurements, which implies that only discrete values (about 12 in each test) of the minimum diameter are available. Again it is found that the results obtained with the finite element model are in good agreement with the experimental data. In particular, it is noted that the time at failure initiation is well predicted.

Figure 5(d) presents the fracture strain from experiments and simulations. For the test specimens, the fracture strain was calculated as  $\varepsilon_f = \ln(A_0/A_f)$ , where  $A$  is the minimum cross-section area of the specimen;  $A_0$  is the initial value of  $A$ , while  $A_f$  is the value of  $A$  after fracture. For the element models, the fracture radius  $a_f$  was measured as the distance from the symmetry axis to the outermost node at minimum cross section after fracture (not including any eroded nodes at the outer surface). Subsequently, the fracture strain was calculated as  $\varepsilon_f = 2 \ln(a_0/a_f)$ , where  $a_0 = d_0 / 2$  is the initial radius of the specimen at the minimum cross-section. The fracture strain is plotted against the triaxiality parameter  $(\sigma_m/\sigma_{eq})_0$ , defined according to Bridgman's analysis (Hancock and Mackenzie [6]). The triaxiality parameter is  $1/3$  at the surface of the specimen, and increases to its maximum value on the symmetry axis of the specimen

$$(\sigma_m / \sigma_{eq})_0 = \frac{1}{3} + \ln(1 + a_0 / 2R_0)$$

It is seen from Figure 5(d) that the finite element model predicts fracture strains that fall within the scatter band found in the experiments. It should be noted that in the tests, the cross-section became oval-shaped during deformation, while this effect is not accounted for in the LS-DYNA simulations.

The deformed geometry of the notched specimens, as obtained with the digital high-speed camera system from tests with pre-load 20 kN, is compared with results from LS-DYNA simulations in Figure 6. It is clearly demonstrated that the simulations are able to capture the local deformation of the notch against time, including a good prediction of the time to fracture. Close-ups of the deformed geometry at fracture initiation from the simulations are presented in Figure 7. It is noted that element erosion starts in the centre of the notch for the notch radii 0.8 mm and 2.0 mm, while it starts at the surface for notch radius 0.4 mm. This observation is in agreement with experimental observations (Holland et al [17]), showing that the fracture process initiates in the central region of the notch for large and medium notch radii, while for small notch radii variations in the plastic strains across the minimum cross-section may lead to fracture initiation at the surface in the notch root.

## Concluding remarks

A validation study has been performed comparing LS-DYNA analyses of notched specimens subjected to impact loading with experimental results obtained in a Split Hopkinson Tension Bar. In the LS-DYNA simulations, a coupled model of viscoplasticity and ductile damage was applied and combined with element erosion to predict failure. Good agreement is obtained between experimentally obtained and predicted curves of force versus elongation, and strain versus time. In addition, both the time at fracture initiation and the fracture strains are well predicted.

## References

- [1] T. Børvik, O.S. Hopperstad, T. Berstad and M. Langseth, “A Computational model of viscoplasticity and ductile damage for impact and penetration”, accepted for publication in *European Journal of Mechanics – A/Solids*, 2001.
- [2] T. Børvik, M. Langseth, O.S. Hopperstad and K.A. Malo, “Ballistic penetration of steel plates, *International Journal of Impact Engineering*, 22, 855-887, 1999.
- [3] T. Børvik, O.S. Hopperstad, T. Berstad and M. Langseth, “Numerical simulation of plugging failure in ballistic penetration”, accepted for publication in *International Journal of Solids and Structures*, 2001.
- [4] T. Børvik, M. Langseth, O.S. Hopperstad and K.A. Malo, “Effect of projectile nose shape in structural impact, Part I: Experimental study”, submitted for publication, 2000.
- [5] T. Børvik, O.S. Hopperstad, T. Berstad and M. Langseth, “Effect of projectile nose shape in structural impact, Part II: Numerical simulations”, submitted for publication, 2000.
- [6] J.W. Hancock and A.C. Mackenzie, “On the mechanisms of ductile failure in high-strength steels subjected to multi-axial stress-states”, *Journal of the Mechanics and Physics of Solids*, 24, 147-169, 1976.
- [7] G.R. Johnson and W.H. Cook, “A constitutive model and data for metals subjected to large strains, high strain rates and high temperatures”, In: *Proceedings of the 7th International Symposium on Ballistics*, The Hague Netherlands, 541-547, 1983.
- [8] F.J. Zerilli and R.W. Armstrong, “Dislocation-mechanics-based constitutive relations for material dynamics calculations”, *Journal of Applied Physics*, 61, 1816-1825, 1987.
- [9] J. Harding, “The development of constitutive relationships for material behaviour at high rates of strain”, *Inst. Phys. Conf. Ser. No 102, Session 5*, 189-202.
- [10] G.T. Camacho and M. Ortiz, “Adaptive Lagrangian Modelling of Ballistic Penetration of Metallic Targets”, *Int. J. Comp. Meth. Appl. Mech. Engng.*, 142, 269-301, 1997.
- [11] G.R. Johnson and W.H. Cook, “Fracture characteristics of three metals subjected to various strains, strain rates, temperatures, and pressures”, *Engineering Fracture Mechanics*, 21, 31-48, 1985.
- [12] J.R. Rice and D.M. Tracey, “On the ductile enlargement of voids in triaxial stress fields”, *Journal of the Mechanics and Physics of Solids*, 17, 210-217, 1969.
- [13] J. Lemaitre, “A course on damage mechanics”, Springer-Verlag, 1992.
- [14] C. Albertini and M. Montagnani, “Testing techniques based on the split Hopkinson bar”, *Inst. Phys. Conf. Ser. No 21*, 1974.
- [15] H. Kolsky, “Stress waves in solids”, Clarendon Press, Oxford, 1953.
- [16] LS-DYNA User’s Manuals, Version 950, Livermore Software Technology Corporation, 1999.
- [17] D. Holland, A. Halim and W. Dahl, “Influence of stress triaxiality upon ductile crack propagation”, *Steel Research*, 61, 504-506, 1990.

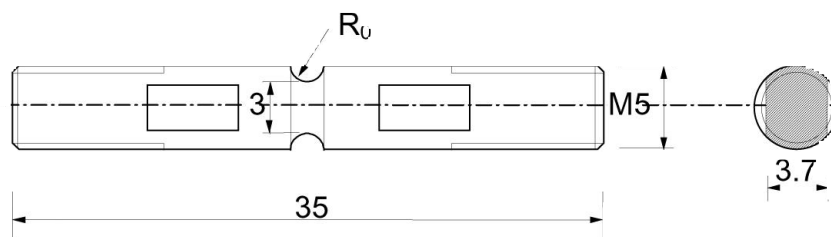


**Figure 1.** Geometry and dimensions of notched specimens (in mm). (Note: For  $R_0 = 0.4$  mm and  $R_0 = 0.8$  mm the side faces of the notch were inclined at an angle of  $17.5^\circ$  to the specimen axis, while for  $R = 2.0$  mm the side faces were normal to the specimen axis (see Figure 3)).

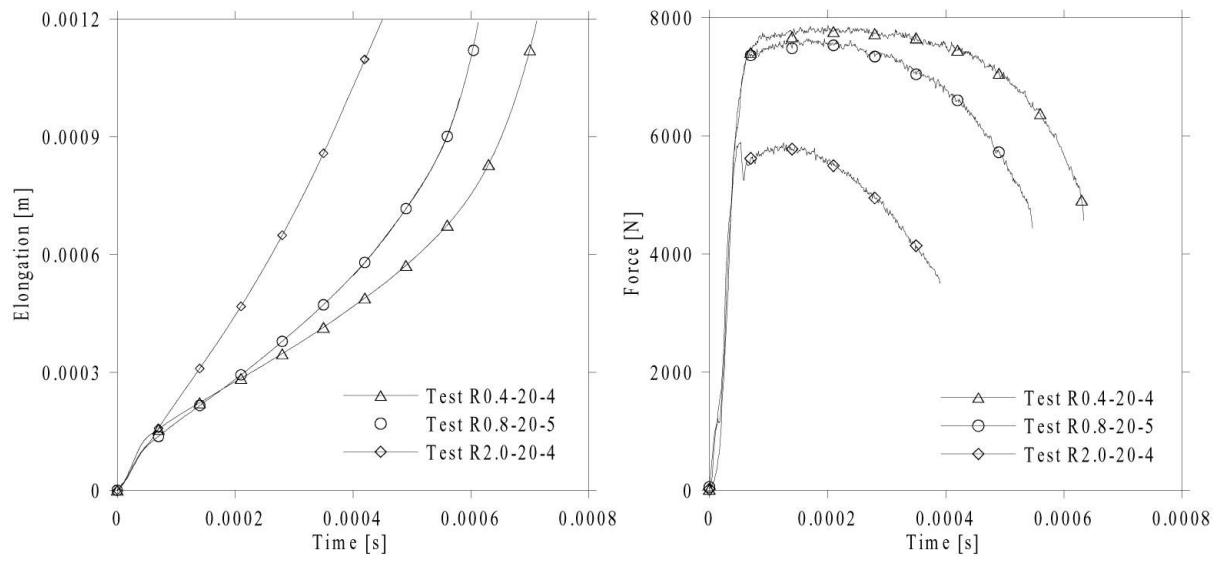


**Figure 2.** Typical elongation-time curves and force-time curves measured in the tests.

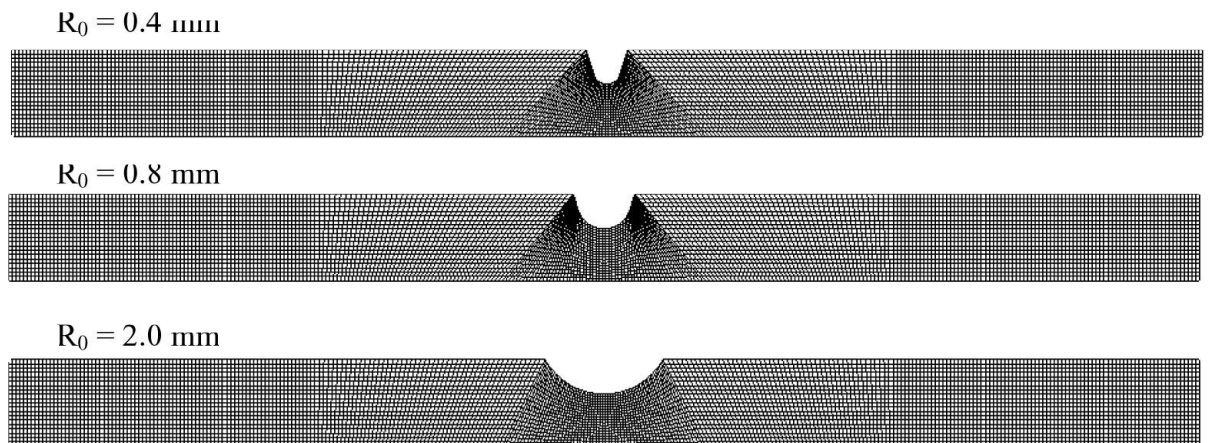
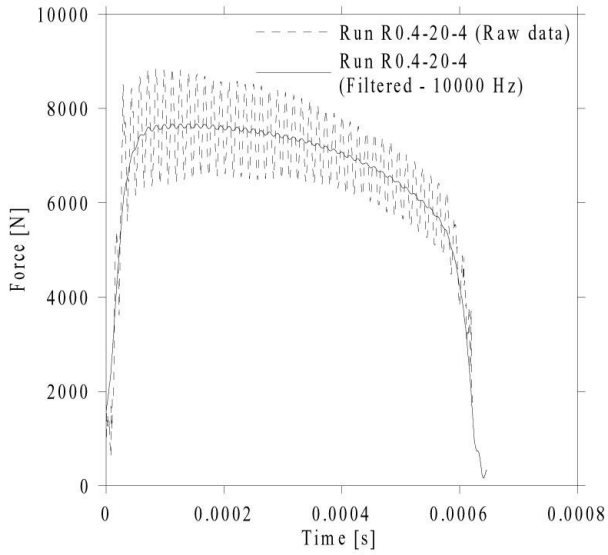
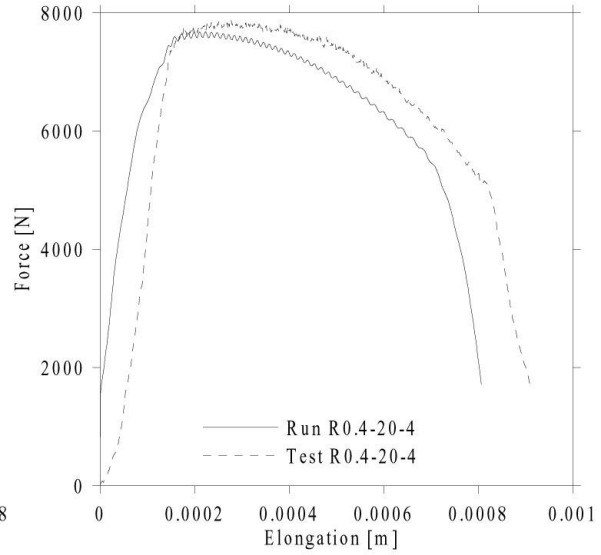


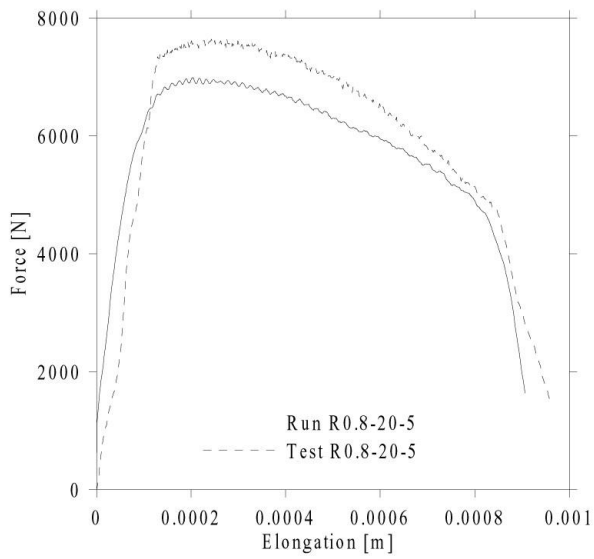
**Figure 3.** Finite element meshes for notched specimens.



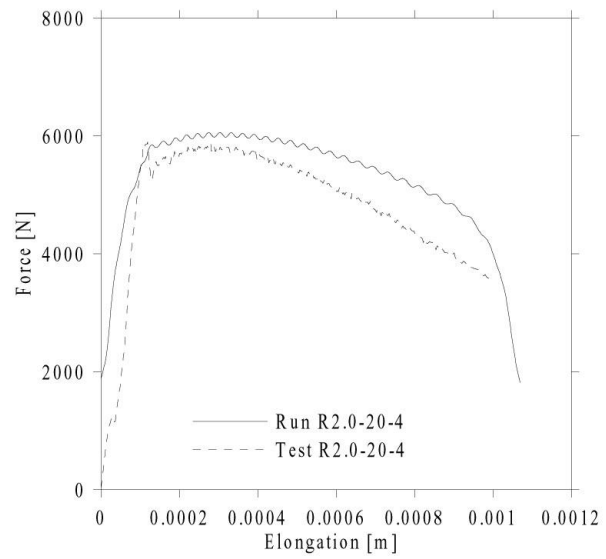
(a)



(b)



(c)



(d)

**Figure 4.** (a) Force-time curve from simulation – raw data and filtered signal; (b)-(d) Force-elongation curves from experiments and simulations.

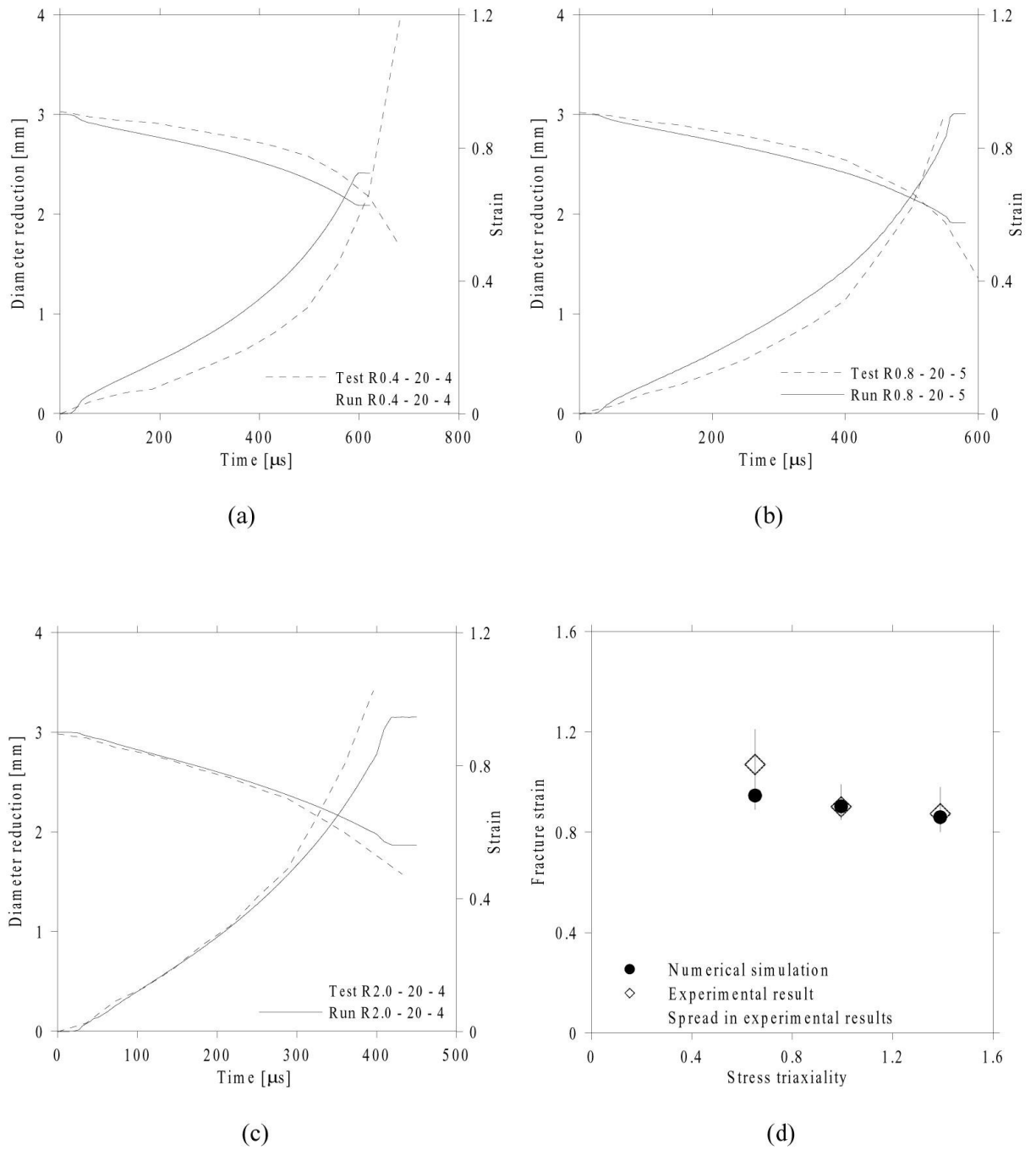
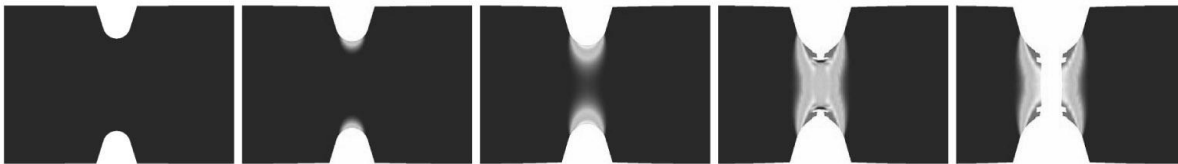
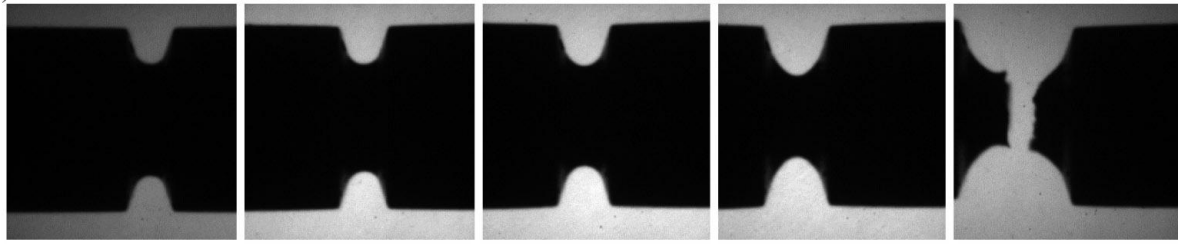


**Figure 5.** (a)-(c) Diameter reduction and strain against time from experiments and simulations; (d) Fracture strain from experiments and simulations.

a) Test R0.4-20-4



$t = 62 \mu\text{s}$

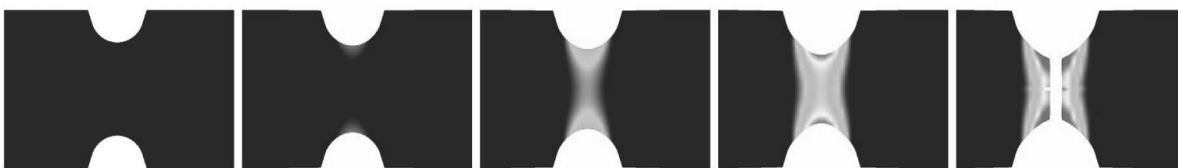
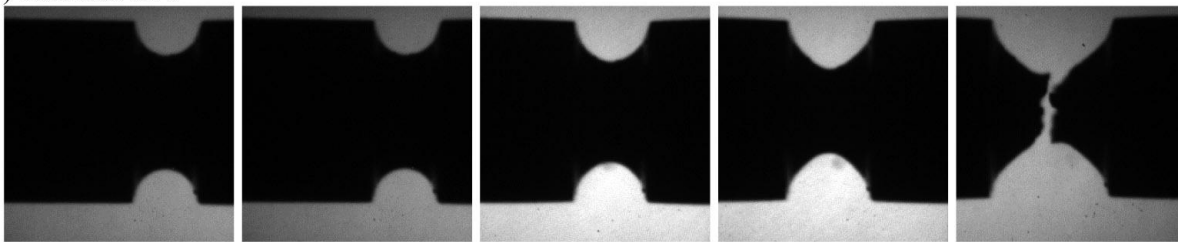
$t = 248 \mu\text{s}$

$t = 434 \mu\text{s}$

$t = 620 \mu\text{s}$

$t = 806/722 \mu\text{s}$

b) Test R0.8-20-5



$t = 50 \mu\text{s}$

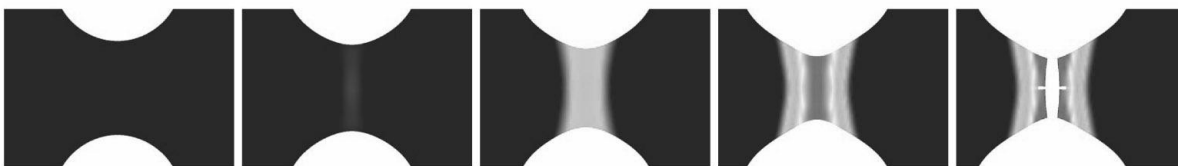
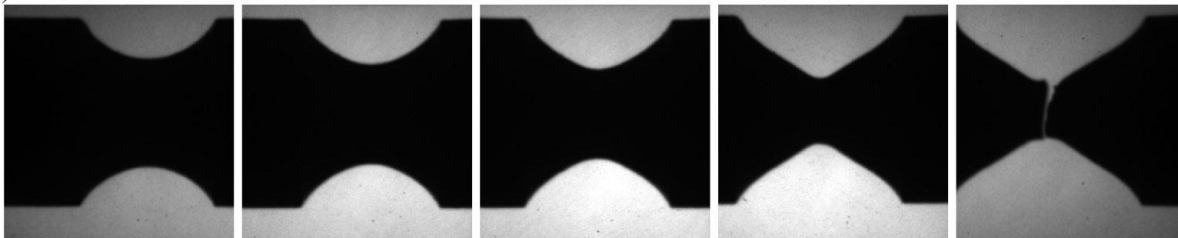
$t = 200 \mu\text{s}$

$t = 350 \mu\text{s}$

$t = 500 \mu\text{s}$

$t = 650/581 \mu\text{s}$

c) Test R2.0-20-4



$t = 36 \mu\text{s}$

$t = 144 \mu\text{s}$

$t = 252 \mu\text{s}$

$t = 396 \mu\text{s}$

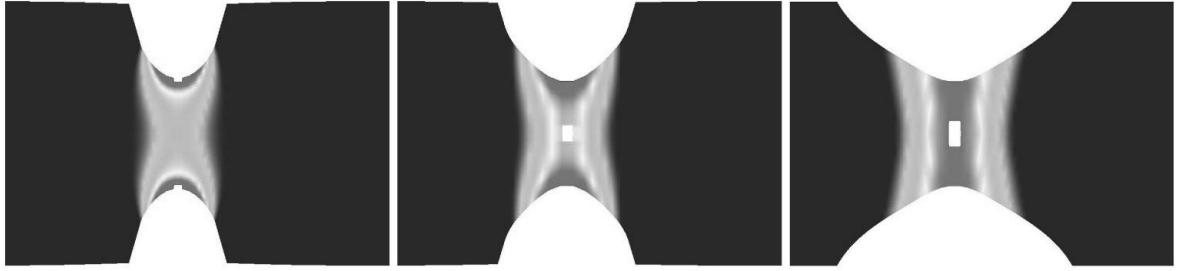
$t = 504/450 \mu\text{s}$

Fringe levels of accumulated plastic strain:

test | simulation



**Figure 6.** A selection of typical high-speed camera images from the tests compared to deformed geometry from simulations showing notch deformation against time.



R=0.4 mm ( $t_i = 592 \mu\text{s}$ ,  $t_f = 621 \mu\text{s}$ ), R=0.8 mm ( $t_i = 552 \mu\text{s}$ ,  $t_f = 564 \mu\text{s}$ ), R=2.0 mm ( $t_i = 401 \mu\text{s}$ ,  $t_f = 423 \mu\text{s}$ )

**Figure 7.** Fracture initiation in simulations ( $t_i$  = time at fracture initiation;  $t_f$  = time at complete fracture).

Table 1. Material constants for Weldox 460 E steel [1].

Elastic constants and density			Yield stress and strain hardening			Strain-rate hardening		Damage evolution		
E (GPa)	$\nu$	$\rho$ (kg/m <sup>3</sup> )	A (MPa)	B (MPa)	n	$\dot{p}_0$ (s <sup>-1</sup> )	C	$D_c$	$p_d$	
200	0.33	7850	490	807	0.73	$5 \cdot 10^{-4}$	0.0114	0.30	0	
Adiabatic heating and temperature softening						Fracture strain constants				
$C_p$ (J/kgK)	$\chi$	$\alpha$ (K <sup>-1</sup> )	$T_m$ (K)	$T_0$ (K)	m	$D_1$	$D_2$	$D_3$	$D_4$	$D_5$
452	0.9	$1.1 \cdot 10^{-5}$	1800	293	0.94	0.0705	1.732	-0.54	-0.015	0